

On the origin of excess cool gas in quasar host halos

Sean D. Johnson^{1*}, Hsiao-Wen Chen¹, and John S. Mulchaey²

¹*Department of Astronomy & Astrophysics and Kavli Institute for Cosmological Physics, The University of Chicago, Chicago, IL 60637, USA*

²*The Observatories of the Carnegie Institution for Science, 813 Santa Barbara Street, Pasadena, CA 91101, USA*

2 September 2021

ABSTRACT

Previous observations of quasar host halos at $z \approx 2$ have uncovered large quantities of cool gas that exceed what is found around inactive galaxies of both lower and higher masses. To better understand the source of this excess cool gas, we compiled an exhaustive sample of 195 quasars at $z \approx 1$ with constraints on chemically enriched, cool gas traced by Mg II absorption in background quasar spectra from the Sloan Digital Sky Survey. This quasar sample spans a broad range of luminosities from $L_{\text{bol}} = 10^{44.4}$ to $10^{46.8}$ erg s⁻¹ and allows an investigation of whether halo gas properties are connected with quasar properties. We find a strong correlation between luminosity and cool gas covering fraction. In particular, low-luminosity quasars exhibit a mean gas covering fraction comparable to inactive galaxies of similar masses, but more luminous quasars exhibit excess cool gas approaching what is reported previously at $z \approx 2$. Moreover, 30 – 40% of the Mg II absorption occurs at radial velocities of $|\Delta v| > 300$ km s⁻¹ from the quasar, inconsistent with gas bound to a typical quasar host halo. The large velocity offsets and observed luminosity dependence of the cool gas near quasars can be explained if the gas arises from: (1) neighboring halos correlated through large-scale structure at Mpc scales, (2) feedback from luminous quasars, or (3) debris from the mergers thought to trigger luminous quasars. The first of these scenarios is in tension with the lack of correlation between quasar luminosity and clustering while the latter two make distinct predictions that can be tested with additional observations.

Key words: quasars: general – galaxies: Seyfert – quasars: absorption lines

1 INTRODUCTION

In order to reproduce the low stellar-to-halo mass ratios of high mass galaxies (e.g. Conroy & Wechsler 2009; Behroozi et al. 2013; Kravtsov et al. 2014) both semi-analytic (e.g. Benson et al. 2003) and hydrodynamic simulations of galaxy evolution must incorporate strong feedback from active galactic nuclei (AGN) and quasars (for a recent review, see Kravtsov & Borgani 2012). Moreover, hydrodynamic simulations of galaxy evolution that incorporate AGN feedback are better able to reproduce the properties of galaxies observed in emission (e.g. Springel et al. 2005; Di Matteo et al. 2005; Sijacki et al. 2007; Schaye et al. 2010; Gabor & Davé 2012; Vogelsberger et al. 2013; Li & Bryan 2014). While promising, these implementations of quasar feedback are subject to significant systematic uncertainties driven by poorly constrained aspects of quasar and AGN physics, and direct observations of quasar feedback are available for only a small number of systems (for a recent review, see Fabian 2012).

The low-density gas of the circum-galactic medium

(CGM) provides a sensitive laboratory for discriminating between possible feedback models, and different feedback prescriptions result in order-of-magnitude changes in CGM observables predicted in hydrodynamic simulations of galaxies (Hummels et al. 2013; Ford et al. 2013; Shen et al. 2013a; Agertz & Kravtsov 2015; Suresh et al. 2015). The density of the CGM is nearly always too low to be studied in emission with existing facilities, but significant progress can be made by studying the gas in absorption when bright background objects are serendipitously found at low projected distances, d , from foreground galaxies.

Over the last decade, large samples totaling nearly one thousand galaxies at $z \approx 0$ to 2 with constraints on extended gas properties from absorption spectroscopy have been assembled using a combination of ground and space-based telescopes. In particular, observations of the H I Lyman series (e.g. Chen et al. 1998; Tripp et al. 1998; Wakker & Savage 2009; Stocke et al. 2013; Rudie et al. 2013; Tumlinson et al. 2013) and doublet transitions due to heavy element ions such as Mg II (e.g. Bowen et al. 1995; Chen et al. 2010a; Gauthier et al. 2010; Bordoloi et al. 2011; Lovegrove & Simcoe 2011), CIV (e.g. Chen et al. 2001; Borthakur et al. 2013; Liang & Chen 2014; Bordoloi et al. 2014), and O VI (e.g. Chen

* E-mail: seanjohnson@uchicago.edu

& Mulchaey 2009; Wakker & Savage 2009; Prochaska et al. 2011; Tumlinson et al. 2011; Mathes et al. 2014; Stocke et al. 2014; Turner et al. 2014; Johnson et al. 2015) have been particularly fruitful.

Recently, observing campaigns leveraging large imaging and spectroscopic surveys such as the Sloan Digital Sky Survey (SDSS; York et al. 2000) and dedicated campaigns on large, ground-based telescopes have extended the study of the relationship between galaxy and halo gas properties to galaxies hosting quasars using projected quasar-quasar pairs. Foreground quasars at both $z \approx 1$ and $z > 2$ exhibit a high incidence of optically thick, metal-enriched absorption systems traced by H I Ly α , C II, C IV, and Mg II absorption along the transverse direction at $d \lesssim 300$ kpc but low incidence along the foreground quasar sightline itself (Bowen et al. 2006; Hennawi et al. 2006; Hennawi & Prochaska 2007; Farina et al. 2013; Hennawi & Prochaska 2013; Prochaska et al. 2013; Farina et al. 2014; Prochaska et al. 2014). This contrast indicates that the ionizing emission from quasars is highly anisotropic, in qualitative agreement with the unified theory of AGN (e.g. Antonucci 1993; Netzer 2015).

The high incidence of optically thick gas at $d < 300$ kpc from quasars at $z \approx 2$ is in significant excess relative to that found for inactive galaxies both at $z < 1$ (Chen et al. 2010a; Gauthier et al. 2010; Lovegrove & Simcoe 2011) and at $z \approx 2$ (Rudie et al. 2012). Insights into the possible origin of this excess gas can be gained from state-of-the-art hydrodynamic simulations that include stellar but not AGN feedback (e.g. Fumagalli et al. 2014). In particular, simulations with stellar feedback are able to comfortably reproduce the observed incidence of Lyman-limit systems around inactive, Lyman-break galaxies at $z \approx 2$ but under-predict the incidence around quasar hosts by more than a factor of two (Faucher-Giguère et al. 2015). This discrepancy suggests that AGN feedback may be responsible for the excess observed in absorption around quasar hosts. Alternatively, the discrepancy could be the result of an inability of the simulations to resolve the physical scales relevant to the formation or survival of cool gas clouds in massive halos (Fumagalli et al. 2014; Meiksin et al. 2015) or if a substantial portion of the gas arises in less luminous galaxies neighboring the quasar hosts (Rahmati et al. 2015; Suresh et al. 2015).

To better understand the relationship between AGN activity and halo gas, we searched the SDSS Data Release 12 (Eisenstein et al. 2011; Alam et al. 2015) and compiled an exhaustive sample of 195 quasars at $z \approx 1$ with constraints on Mg II absorption at $d < 300$ kpc from background quasars. This large dataset enables a search for correlations between quasar properties and extended, cool circumgalactic gas around the quasar hosts.

The paper proceeds as follows: In Section 2 we describe the quasar sample and corresponding absorption-line measurements. In Section 3, we characterize the absorption as a function of projected distance, redshift, and quasar luminosity. In Section 4, we discuss the implications of our findings.

Throughout the paper, we adopt a Λ -cosmology with $\Omega_m = 0.3$, $\Omega_\Lambda = 0.7$, and $H_0 = 70 \text{ km s}^{-1} \text{ Mpc}^{-1}$. All magnitudes are in the AB system (Oke & Gunn 1983) and corrected for foreground Milky Way extinction following Schlafly & Finkbeiner (2011).

2 QUASAR SAMPLE

To compile a large sample of foreground-background quasar¹ pairs with constraints on Mg II absorption, we retrieved a list of the 395,281 quasars classified by the SDSS-III automated classification and redshift measurement pipeline (Bolton et al. 2012) as of Data Release 12. From this sample, we selected foreground-background quasar pairs that meet the following criteria:

- (i) The projected distance between the foreground and background quasars at the foreground quasar redshift satisfies $d < 300$ kpc.
- (ii) The velocity difference between the foreground and background quasars satisfies $\Delta v(z_b, z_f) < -10,000 \text{ km s}^{-1}$.
- (iii) The expected wavelengths of the Mg II doublet at the redshift of the foreground quasar is covered by the SDSS spectrum of the background quasar.
- (iv) The expected wavelengths of the Mg II doublet is outside of the Ly α forest in the background quasar spectrum.
- (v) The signal-to-noise ratio in the background quasar spectrum is sufficient to detect a moderate strength Mg II absorption system with rest-frame equivalent width of $W_r(2796) > 0.3 \text{ \AA}$ at $3\text{-}\sigma$ significance at the foreground quasar redshift (a signal-to-noise ratio of 20 per SDSS resolution element).

The upper limit on the projected distance was chosen to correspond to the expected virial radii of quasar host halos at $z > 0.4$. The requirement that $\Delta v < -10,000$ was chosen to avoid confusion with gas outflowing from the background quasar (e.g. Wild et al. 2008). The requirement that the wavelengths of the Mg II doublet at the foreground quasar redshift fall outside of the Ly α forest in the background quasar spectrum was chosen to ensure that absorption attributed to Mg II is not the result of coincidental Ly α absorption systems. Finally, the requirement that the signal-to-noise ratio in the background quasar spectrum is sufficient to detect absorption systems of $W_r(2796) > 0.3 \text{ \AA}$ was chosen to correspond to the typical sensitivities of existing studies of Mg II absorption around quasars at $z \approx 1$ (e.g. Farina et al. 2013, 2014).

The search yielded a sample of 195 foreground-background quasar pairs which we visually inspected to ensure that the automated classifications as broad-line (Type 1) quasars and redshifts from the SDSS database are robust. For each of the 195 quasar pairs, we then measured foreground quasar properties and Mg II absorption properties as described in Sections 2.1 and 2.2 respectively. The sample is summarized in Table 1.

2.1 Foreground quasar redshifts and luminosities

Quasar redshifts from the SDSS pipeline are biased by $\approx 600 \text{ km s}^{-1}$ due to asymmetric, blue-shifted emission profiles of broad-line region emitting gas (Gaskell 1982; Tytler & Fan 1992; Richards et al. 2002; Hewett & Wild 2010). This

¹ Throughout this paper, we refer to objects with broad-line emission and power-law dominated continua as quasars irrespective of the sub-division of AGN into quasars and Seyferts based on luminosity.

Table 1. Summary of quasar and absorption properties. The full table is available in the on-line version of the paper.

Name	Foreground quasar				$\Delta\theta$ ($''$)	d (kpc)	Absorption properties		Ref. ^c
	Right Ascension (J2000)	Declination (J2000)	z^a	$\log L_{\text{bol}}/\text{erg s}^{-1}$			$W_r(2796)^b$ (\AA)	Δv (km s^{-1})	
J0954+3734	09:54:54.70	+37:34:19.7	1.544	46.3	3.1	26	1.10 ± 0.17	660	1
J0836+4841	08:36:49.40	+48:41:50.0	0.657	45.7	4.1	28	1.90 ± 0.11	-130	1
J0842+4733	08:42:57.37	+47:33:42.6	1.556	46.5	3.4	29	3.70 ± 0.30	-790	4
J1550+1120	15:50:43.59	+11:20:47.5	0.4358	46.0	5.2	29	< 0.25	n/a	4
J1106+4635	11:06:17.17	+46:35:24.5	1.602	46.5	4.4	37	1.12 ± 0.15	-130	4
J1108+3306	11:08:07.90	+33:06:11.3	1.502	46.5	5.5	46	5.75 ± 0.26	810	4
J0938+5317	09:38:04.21	+53:17:43.9	2.063	45.9	5.7	47	0.48 ± 0.04	310	3
J2312+1444	23:12:52.70	+14:44:58.6	0.7678	45.2	6.4	47	0.39 ± 0.12	-100	1
J1427-0121	14:27:58.88	-01:21:30.3	2.281	46.6	6.2	51	0.45 ± 0.02	-80	3
J0909+1629	09:09:57.08	+16:29:06.5	0.7275	45.2	7.1	51	< 0.15	n/a	4

Notes

^a Quasars with redshifts from narrow [O II] or [O III] are shown to four decimal places and three decimal places otherwise.

^b For non-detections, we report 3- σ upper limits integrated over a 250 km s^{-1} velocity interval.

^c Reference: 1 \rightarrow Bowen et al. (2006), 2 \rightarrow Farina et al. (2013, 2014), 3 \rightarrow Prochaska et al. (2014), 4 \rightarrow This work

bias exceeds the velocity difference typically found between galaxies and associated Mg II absorption at $d < 150$ kpc (Chen et al. 2010a) so more accurate redshifts are required. When available, we adopted redshifts from Hewett & Wild (2010) and otherwise, we calculated the quasar redshifts using the template and cross-correlation techniques described in Hewett & Wild (2010). In addition, for quasars with narrow [O II] or [O III] emission, we measured the redshifts from these narrow emission lines by fitting gaussian profiles and adopting the rest-frame line centroid wavelengths from Hewett & Wild (2010).

Uncertainties in narrow-line based redshifts due to centroid uncertainties are typically small, $\sigma \approx 30 \text{ km s}^{-1}$, but [O III] redshifts can be blueshifted due to outflows in the narrow-line region (Boroson 2005). To evaluate the significance of this bias, we compared [O II] and [O III] emission redshifts for quasars within our SDSS sample and found a mean bias of $\Delta v(z_{\text{O II}}, z_{\text{O III}}) = -30 \text{ km s}^{-1}$ with a 1- σ scatter of 70 km s^{-1} .

Broad-line based cross-correlation redshifts exhibit larger scatter with significant, non-Gaussian wings in the redshift error distribution due to population variance in broad-line profiles. To evaluate the uncertainties in our broad-line based redshifts, we remeasured the cross-correlation redshifts for quasars with narrow-line emission but with the narrow-lines masked during the cross-correlation. We then compared these broad-line redshifts with the narrow-line redshifts. The bias in the broad-line based cross-correlation redshifts is consistent with zero and the 68%, 95%, 99%, and 99.7% uncertainties correspond to 150, 370, 1000, and 1500 km s^{-1} respectively.

In addition to improved redshifts, we measured quasar bolometric luminosities based on monochromatic, continuum luminosity measurements and the bolometric corrections from Richards et al. (2006). The monochromatic luminosities were estimated by fitting a power-law continuum plus Fe II template (Vestergaard & Wilkes 2001) model to line-free continuum regions of the SDSS quasar spectra with rest-frame wavelength intervals of $\lambda_r = 1350 - 1360, 1445 - 1465, 1700 - 1705, 2155 - 2400, 2480 - 2675, \text{ and } 2925 - 3500 \text{ \AA}$. The uncertainties in the quasar bolometric luminosities

are dominated by sample variance in quasar spectral energy distributions which result in errors of ≈ 0.3 dex (see discussion in Richards et al. 2006).

In order to include previously reported quasars with absorption line constraints at $d < 300$ kpc, we measured bolometric luminosities for quasars from Bowen et al. (2006); Farina et al. (2013, 2014) and Prochaska et al. (2014) with available SDSS spectra using the same techniques. For the quasars from Farina et al. (2013) and Farina et al. (2014) without SDSS spectra we adopted the bolometric luminosity estimates reported by Farina et al. (2013) and Farina et al. (2014) which were measured using a similar continuum fitting procedure. For those quasars from Bowen et al. (2006) and Prochaska et al. (2014) without public spectra, we estimated luminosities by finding close matches in redshift and apparent magnitude space in the quasar sample from Shen et al. (2011) which has monochromatic luminosities estimated from continuum fitting. These broad-band based luminosities reproduce spectroscopic measurements with a standard deviation of 0.2 dex.

The redshift, luminosity, and projected distance distributions of the resulting quasar catalogs are displayed in the Figure 1. The samples from Bowen et al. (2006), Farina et al. (2013), Farina et al. (2014), and this work are characterized by mean redshifts of $\langle z \rangle \approx 1$ while the sample from Prochaska et al. (2014) is characterized by $\langle z \rangle = 2.2$. The quasar sample presented in this paper spans a luminosity range of $\log L_{\text{bol}}/\text{erg s}^{-1} = 44.4$ to 46.8 (see the left panel of Figure 1), extending the study of gas in absorption around quasars to lower luminosities than were previously available.

2.2 Absorption-line measurements

In order to place constraints on the transverse Mg II absorption near the foreground quasars, we visually searched the background quasar spectra for possible Mg II $\lambda 2796$ absorption within $|\Delta v| < 1500 \text{ km s}^{-1}$ of the foreground quasar redshift. The large search window was chosen to ensure that uncertainties in broad-line based quasar redshifts do not bias the results of this study. In addition, this velocity search window is the same as was used by Prochaska

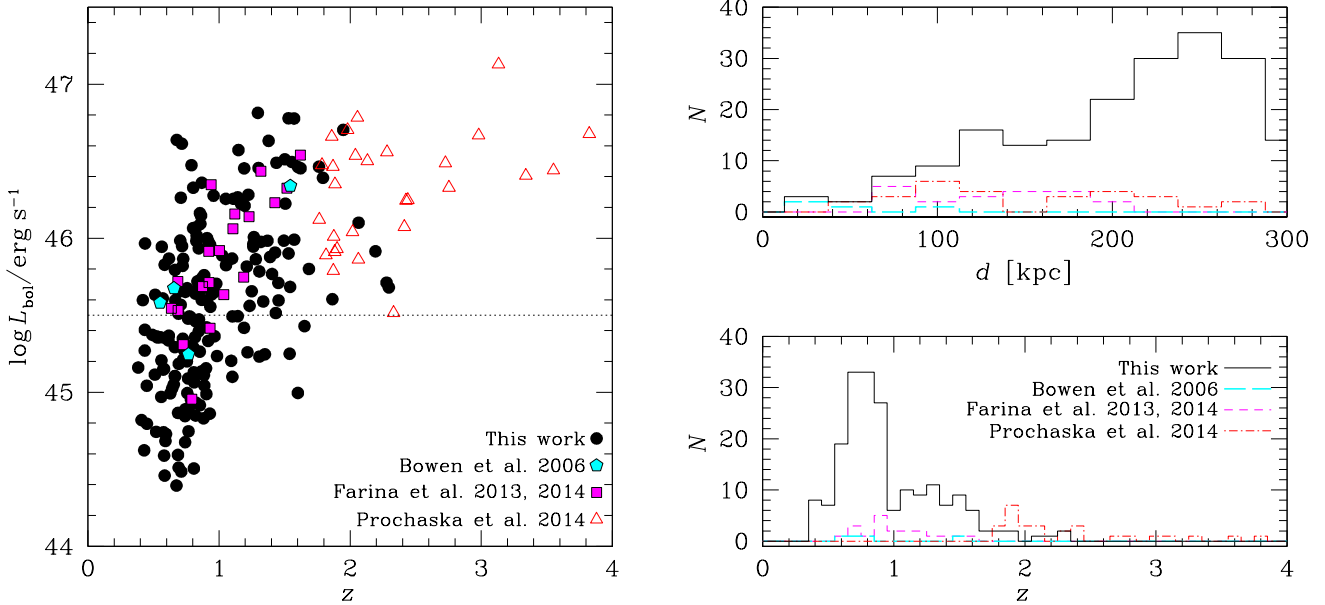


Figure 1. *left:* Bolometric luminosity of the foreground quasars versus foreground quasar redshift. The horizontal dotted line marks $\log L_{\text{bol}}/\text{erg s}^{-1} = 45.5$, the division between the luminous and low-luminosity quasars used throughout the paper. *right:* Projected distance (*top*) and redshift (*bottom*) histograms. In all three panels, quasars from Bowen et al. (2006), Farina et al. (2013) or Farina et al. (2014), Prochaska et al. (2014), and this work are displayed in cyan, magenta, red, and black respectively, with symbols and line-styles indicated in the legend. The quasars from Bowen et al. (2006), Farina et al. (2013), Farina et al. (2014), and this work have available constraints on the transverse Mg II absorption from the spectra of background quasars. Mg II absorption constraints are unavailable for the quasar sample from Prochaska et al. (2014) due to the higher redshift range. For these quasars, C II rather than Mg II serves as a signature of cool, high HI column density gas.

et al. (2014) which simplifies the comparison between that work and our $z \approx 1$ sample.

When absorption was identified, we measured the absorption equivalent width and centroid in the following steps. First, we locally fit the continuum by defining feature-free continuum regions at lower and higher wavelengths and fit an outlier-resistant line to these continuum regions. We then continuum normalized the flux and error arrays and calculated the rest-frame equivalent width and equivalent width error by direct integration over a user-defined interval. We accepted the absorption according to a $3\text{-}\sigma$ detection threshold and additionally required that the identification of the absorption feature as Mg II $\lambda 2796$ be confirmed by the presence of at least one other absorption feature at the same redshift (e.g. Mg II $\lambda 2803$, Mg I $\lambda 2852$, or Fe II $\lambda\lambda 2344, 2374, 2382, 2586, 2600$). Finally, we measured the absorber centroid and full-width-at-half-maximum (FWHM) by fitting a gaussian profile to the Mg II $\lambda 2796$ absorption and used the centroid to measure the absorber redshift. In a few cases, multiple absorption components are found at $|\Delta v| < 1500 \text{ km s}^{-1}$. For these quasars, we report the total Mg II $\lambda 2796$ equivalent width and report Δv for the strongest component. Each of these cases is discussed further in Section 3.2.

In the case of non-detections, we placed $3\text{-}\sigma$ upper limits on the Mg II $\lambda 2796$ equivalent width by integrating the continuum normalized error array over a 250 km s^{-1} window centered at the foreground quasar redshift. The 250 km s^{-1} window corresponds to the mean FWHM of Mg II $\lambda 2796$ detections in our sample. Two example quasars probed in ab-

sorption, one with detected Mg II absorption and one without, are showcased in Figure 2 to demonstrate the data quality afforded by the SDSS spectra.

In one case, J1250–0105, we identified possible Mg II $\lambda 2796$ absorption with $3\text{-}\sigma$ significance but were unable to confirm the identification by detection of another line. For this quasar, we placed a limit on the Mg II $\lambda 2796$ equivalent width by measuring the limit on Mg II $\lambda 2803$ and multiplied by two (the ratio of the oscillator strengths of the two transitions). We note that the results presented in this paper do not change if the possible Mg II $\lambda 2796$ absorption for this quasar is treated as a detection.

In a few cases, we detected absorption from the Mg II doublet but with the $\lambda 2796$ member contaminated by heavy element absorption from another absorption system at a distinct redshift. For these objects, we fitted the Mg II and contaminating absorption profiles using the VPFIT package (Carswell et al. 1987; Carswell & Webb 2014) and measured Mg II $\lambda 2796$ equivalent width from the model fit.

Finally, we added absorption-line measurements from the foreground-background quasar samples previously reported in the literature in Bowen et al. (2006); Farina et al. (2013, 2014), and Prochaska et al. (2014). The sample from Bowen et al. (2006) contains four foreground quasars probed at $d = 26, 29, 47,$ and 98 kpc all of which are detected in Mg II absorption with equivalent widths ranging from $W_r(2796) = 0.4$ to 1.9 \AA . We included quasars from Farina et al. (2013) and Farina et al. (2014) after converting their $2\text{-}\sigma$ detection limits to $3\text{-}\sigma$, applying a uniform cut requiring sufficient signal in the background quasar spectrum

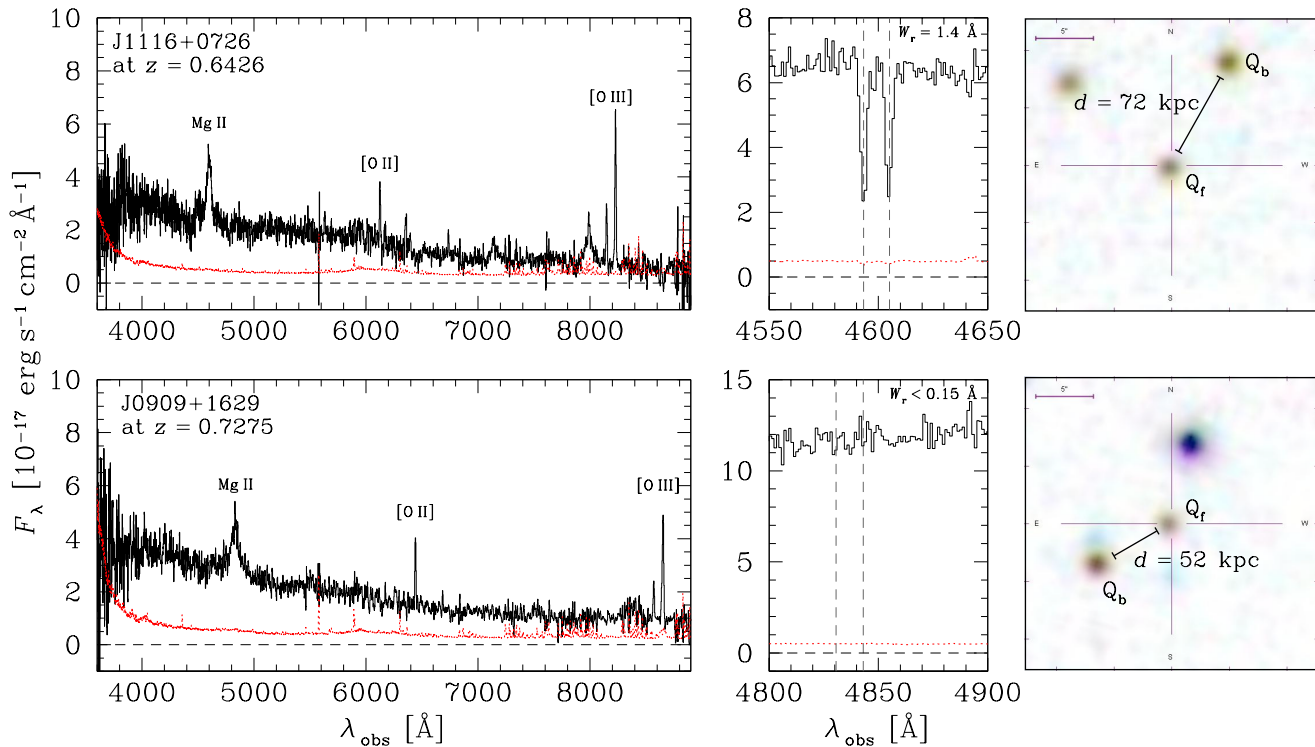


Figure 2. Two example quasars probed in Mg II absorption. The *top* panels display a quasar detected in Mg II absorption at $d = 72$ kpc and the *bottom* panels display a quasar without detected Mg II absorption at $d = 52$ kpc. The *left* panels display the SDSS spectra of the foreground quasars. The *middle* panels display the SDSS spectra of the background quasars with the expected positions of the Mg II doublet members at the systemic redshift of the foreground quasar marked by vertical dashed lines. In both the left and middle panels, the flux and error arrays are shown in black histogram and dotted red line respectively. The zero-flux level is marked by a horizontal, black dashed line. The SDSS image of the fields around the quasars are shown on the *right* with the position of the foreground and background quasars labelled as Q_f and Q_b respectively. The purple line at the top left of each image is $5''$ in length.

to detect an absorption system of $W_r(2796) > 0.3 \text{ \AA}$, and restricting the Mg II search window to $|\Delta v| < 1500 \text{ km s}^{-1}$.

The quasar sample from Prochaska et al. (2014) spans a redshift range of $z = 1.8 - 3.8$, and consequently Mg II absorption constraints are not available with the existing optical spectra. Mg II absorption traces cool ($T \sim 10^4 \text{ K}$) gas (Bergeron & Stasińska 1986) with high HI column densities of $N(\text{HI}) \approx 10^{18} - 10^{22}$ (Rao et al. 2006). At $z \gtrsim 2$, C II $\lambda 1334$ absorption can serve as an alternative tracer of such cool, high column density gas. Neutral Magnesium and Carbon share similar ionization potential and we therefore expect the ratio of Mg II to C II equivalent width to approximately follow the rest-frame wavelength ratios, $W_r(2796)/W_r(1334) = 2.09$ for saturated systems with line-widths dominated by non-thermal broadening. Empirically, low-redshift galaxies with constraints on both Mg II and C II equivalent widths from Werk et al. (2013) exhibit a mean ratio of $W_r(2796)/W_r(1334) = 1.7$. In order to compare the cool gas contents around high redshift quasars with the sample in this work, we adopted this mean ratio to convert from the C II equivalent widths reported in Prochaska et al. (2014) to expected Mg II equivalent widths (consistent with the conversion from Prochaska et al. (2014)). To maintain a uniform cut in absorption sensitivity, we restricted the quasar sample from Prochaska et al. (2014) to those with signal-to-noise in the background spectrum sufficient to detect a C II $\lambda 1334$ absorption system of $W_r(1334) > 0.18$

\AA at $3\text{-}\sigma$ significance. This sensitivity corresponds to the $W_r(2796) > 0.3 \text{ \AA}$ sensitivity requirement adopted for the $z \approx 1$ samples with constraints on Mg II absorption.

3 MG II ABSORPTION NEAR QUASARS

With the quasar and absorption-line measurements described in Section 2 in hand, we characterize the Mg II absorption found around quasars as a function of projected distance, luminosity, and redshift in Section 3.1. In addition, we explore the kinematics of the absorption systems in Section 3.2 and discuss associated Mg II absorption systems found along the sightline to the foreground quasar itself in Section 3.3.

3.1 Dependence on projected distance, luminosity, & redshift

We characterize Mg II equivalent width as a function of projected distance in the left panel of Figure 3 and display the measurements from Bowen et al. (2006); Farina et al. (2013, 2014), and Prochaska et al. (2014) for comparison. The Mg II equivalent widths exhibit an anti-correlation with projected distance that is driven by a decrease in incidence at large projected distances. To verify the significance

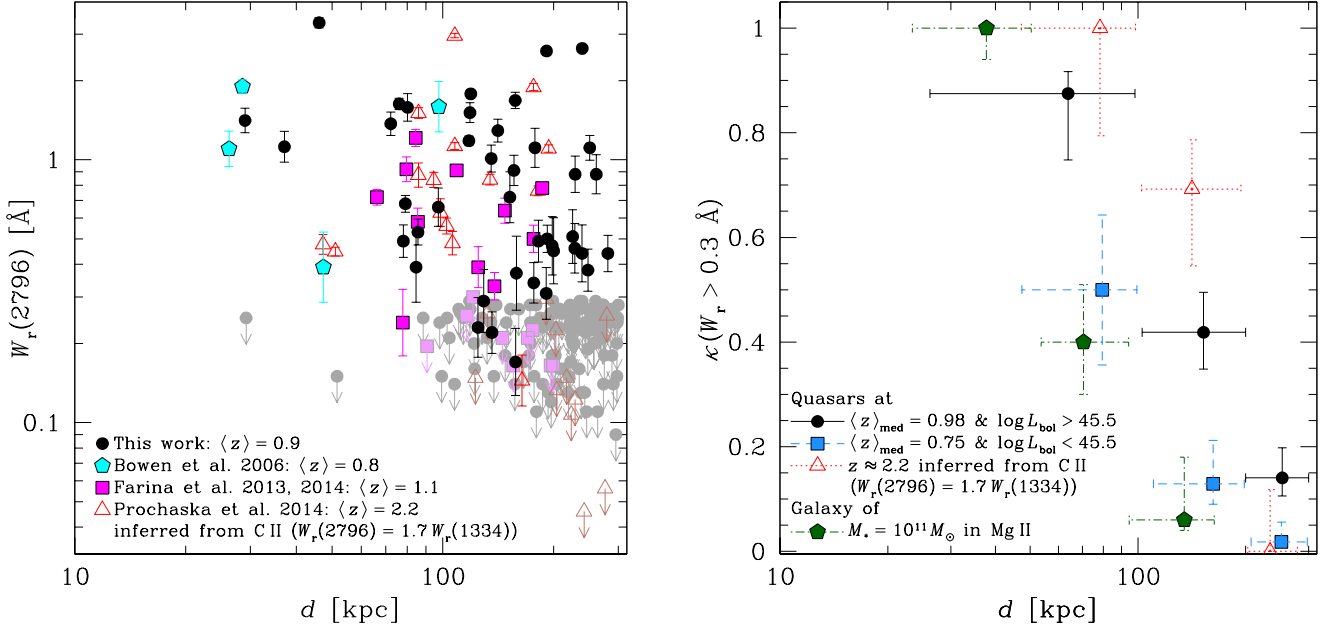


Figure 3. *left:* Rest-frame Mg II $\lambda 2796$ equivalent width versus projected distance. Symbols and coloring are as in Figure 1. Non-detections are shown as $3\text{-}\sigma$ upper limits marked by downward arrows and lighter shading. *right:* Covering fraction for absorption systems with $W_r(2796) > 0.3 \text{ \AA}$ as a function of projected distance for the quasars probed in Mg II with luminous quasars ($\log L_{\text{bol}}/\text{erg s}^{-1} > 45.5$) in black solid line and low-luminosity quasars ($\log L_{\text{bol}}/\text{erg s}^{-1} < 45.5$) in blue dashed line. For comparison, the covering fraction for luminous quasars at $z \approx 2.2$ based on sample probed in C II from Prochaska et al. (2014) is shown in red dotted line. Finally, we also show the expected covering fraction for galaxies with stellar mass $\log M_*/M_\odot = 11$ in green dash-dot line. The vertical error bars mark 68% confidence intervals calculated from binomial statistics with a flat prior ($\kappa \in [0, 1]$) and the horizontal error bars mark the full range of projected distances contributing to each bin. The bins are chosen to span the range of $d = 0 - 300 \text{ kpc}$ in 100 kpc wide intervals. We note that the expected incidence of coincidental Mg II absorption systems unrelated to the quasars within the velocity search window is insignificant ($\kappa_{\text{rand}} = 0.01$) based on the Mg II $\partial N/\partial z \partial W_r$ measurement from Zhu & Ménard (2013). The SDSS quasars are drawn from a flux-limited survey and consequently, the luminous quasars occur at a higher median redshift of $\langle z \rangle_{\text{med}} = 0.98$ compared to $\langle z \rangle_{\text{med}} = 0.75$ for the low-luminosity quasars. The higher gas covering fractions observed for the luminous quasars could therefore be the result of luminosity-dependence, redshift evolution, or a combination of the two. The observed correlation between covering fraction and luminosity is isolated from the possible effects of redshift evolution in Figure 4.

of this anti-correlation between equivalent width and projected distance, we perform a generalized Kendall- τ rank correlation test including the non-detections as upper limits (Isobe et al. 1986). The Kendall test finds an anti-correlation characterized by a coefficient of -0.3 with a high significance of $p \ll 1\%$ ². The anti-correlation is driven primarily by a decrease in the incidence of absorption systems at $d \gtrsim 100 \text{ kpc}$ rather than by a decrease in the mean equivalent width of detections. Interestingly, strong absorption systems of $W_r(2796) > 1.0 \text{ \AA}$ are observed at $d > 100 \text{ kpc}$, in stark contrast to L_* galaxies at $z < 1.5$ (Chen et al. 2010a; Lovegrove & Simcoe 2011).

Using a sample of quasars probed in absorption by background quasar spectra placing constraints on C II absorption, Prochaska et al. (2014) found excess absorption for quasars at $z \approx 2.2$ compared to quasars probed in Mg II at $z \approx 1$ (Farina et al. 2013, 2014). Prochaska et al. (2014) interpreted this excess as redshift evolution in the properties of

quasar host halos. However, the quasars in the $z \approx 2.2$ sample from Prochaska et al. (2014) are characterized by high luminosities (see left panel of Figure 1), and it is not clear that they form a representative sample for the entire quasar population. To investigate this possibility, we combine our SDSS quasars with those reported in the literature with Mg II constraints (Bowen et al. 2006; Farina et al. 2013, 2014) and divide the resulting combined Mg II sample at the median luminosity into luminous quasars of $\log L_{\text{bol}}/\text{erg s}^{-1} > 45.5$ and low-luminosity ones of $\log L_{\text{bol}}/\text{erg s}^{-1} < 45.5$. In doing so, we restrict the combined Mg II quasar sample to those with $z < 1.8$ where the sample follows the well defined redshift-luminosity trend seen in Figure 1. We note that this luminosity division also corresponds to the traditional division of AGN into quasars and Seyfert galaxies (e.g. Schmidt & Green 1983).

Both the luminous and low-luminosity quasars exhibit decreasing covering fraction as a function of projected distance as shown in the right panel of Figure 3. In particular, the low-luminosity quasar covering fraction decreases from $\kappa_{\text{Mg II}} = 0.50 \pm 0.14$ at $d < 100 \text{ kpc}$ to $\kappa_{\text{Mg II}} = 0.13^{+0.08}_{-0.04}$ and $\kappa_{\text{Mg II}} = 0.02^{+0.04}_{-0.01}$ at $d = 100 - 200$ and $200 - 300 \text{ kpc}$ respectively. The Mg II covering fractions for low-luminosity quasars are consistent within uncertainties with expecta-

² We note that the measurement uncertainties will tend to bias the correlation coefficient toward zero and perform this test to estimate the statistical significance of the anti-correlation within our sample rather than to measure the coefficient.

tions for inactive galaxies with stellar masses $\log M_*/M_\odot \approx 11$ based on the covering fraction and stellar mass scaling relation measurements from Chen et al. (2010a) and Chen et al. (2010b)³. A stellar mass of $\log M_*/M_\odot \approx 11$ is chosen for this comparison because it is the expected stellar mass of galaxies with halo masses similar to quasar hosts (Shen et al. 2013b) based on the stellar-to-halo mass relation from Behroozi et al. (2013). On the other hand, the luminous quasars exhibit enhanced covering fraction that are a factor of ≈ 2 or more higher than those of the low-luminosity quasars over the full range of projected distances studied here with $\kappa_{\text{Mg II}} = 0.88^{+0.04}_{-0.13}$ at $d < 100$ kpc, $\kappa_{\text{Mg II}} = 0.42 \pm 0.07$ at $d = 100 - 200$, and $\kappa_{\text{Mg II}} = 0.14^{+0.06}_{-0.03}$ at $d = 200 - 300$.

To verify the significance of the excess Mg II absorption around luminous quasars relative to low-luminosity ones over the full range of projected distances studied here, we also calculate the covering fraction at $d < 300$ kpc for the low-luminosity quasars and luminous quasars and find $\kappa_{\text{Mg II}} = 0.10^{+0.04}_{-0.02}$ and $0.34^{+0.05}_{-0.04}$ respectively. In addition, we perform a logrank test (Feigelson & Nelson 1985) comparing the distributions of the Mg II equivalent widths for the low-luminosity quasars and redshift weighted luminous quasars at $d < 300$ kpc. The logrank tests yields $L_n = 15.2 \pm 3.7$, which confirms that the luminous quasars exhibit excess Mg II absorption relative to low-luminosity quasars with a significance of $p \ll 1\%$.

While the low- and high-luminosity quasars exhibit distinct gas covering fractions, it is possible that the difference in gas covering fraction is the result of redshift evolution in quasar host halo gas properties. In particular, the SDSS quasar sample is drawn from a flux-limited survey, and consequently the luminous quasars in our sample occur a higher median redshift of $\langle z \rangle_{\text{med}} = 0.98$ compared to $\langle z \rangle_{\text{med}} = 0.75$ for the low-luminosity quasars as shown in Figure 1. The excess absorption observed around the luminous quasars could therefore be the result of luminosity dependence, redshift evolution, or a combination of the two. To isolate the luminosity dependence, we restrict the luminous quasar sample to $z < 1$ in order to match the median redshift of the luminous quasar sample to that of the low-luminosity quasars. The covering fraction for the luminous quasars at $z < 1$ and $d < 300$ kpc is $\kappa_{\text{Mg II}} = 0.32^{+0.07}_{-0.05}$ compared to $\kappa_{\text{Mg II}} = 0.10^{+0.04}_{-0.02}$ for the low-luminosity quasars. A logrank test comparing the Mg II equivalent width distribution of the low-luminosity quasars with that of the luminous quasar at $z < 1$ confirms this excess with a significance of $p \ll 1\%$. The comparison of the Mg II absorption incidence between the luminous and low-luminosity quasars with restricted redshift ranges indicates that the observed correlation between covering fraction and luminosity is not being driven by underlying redshift evolution.

The observed correlation between Mg II absorption covering fraction and quasar luminosity can explain a significant portion of the excess cool gas found for quasars at $z \approx 2.2$ relative to those at $z \approx 1$. Nevertheless, the covering frac-

tions for the luminous quasars at $z \approx 1$ probed in Mg II at $d = 100 - 200$ kpc are somewhat lower than those of the $z \approx 2.2$ quasars probed in C II from Prochaska et al. (2014) ($\kappa = 0.69^{+0.09}_{-0.15}$). This possible difference between the $z \approx 1$ and $z \approx 2$ samples could be the result of additional correlation with luminosity, a difference in projected distance distribution between the $z \approx 1$ and $z \approx 2.2$ samples, or evolution in cool gas content of quasar host halos.

To differentiate these possibilities, we plot the covering fraction of Mg II absorption systems with $W_r(2796) > 0.3 \text{ \AA}$ at $d < 200$ kpc as a function of luminosity for the combined Mg II quasar sample after resampling to mimic the flatter projected distance distribution of the Prochaska et al. (2014) sample in the left panel of Figure 4. The resampling is accomplished by randomly resampling the quasars probed in Mg II without replacement to construct a maximal possible sample with the projected distance distribution mimicking that of Prochaska et al. (2014). The random resampling is repeated a large number of times to measure the mean covering fraction. Uncertainties in the mean covering fraction are calculated from binomial statistics with the sample size of the largest possible subsample with flat projected distance distribution.

The low-luminosity quasars ($\log \langle L_{\text{bol}}/\text{erg s}^{-1} \rangle = 45.2$) exhibit a mean covering fraction of $\kappa_{\text{Mg II}} = 0.25^{+0.10}_{-0.06}$ while the luminous ones ($\log \langle L_{\text{bol}}/\text{erg s}^{-1} \rangle = 45.9$) exhibit a covering fraction of $\kappa_{\text{Mg II}} = 0.6^{+0.06}_{-0.07}$ at $d < 200$ kpc, indicating a strong correlation between quasar luminosity and the incidence of extended Mg II absorbing gas. A similar trend of increasing covering fraction with luminosity is observed when the sample is restricted to $z < 1$ (see the blue points in Figure 4). The trend of increasing covering fraction with luminosity found for the $z \approx 1$ quasars connects smoothly with the high covering fractions ($\kappa = 0.76^{+0.07}_{-0.13}$) found for high-luminosity quasars ($\log \langle L_{\text{bol}}/\text{erg s}^{-1} \rangle = 46.2$) at $z \approx 2.2$ from Prochaska et al. (2014) (see the left panel of Figure 4). We note that in calculating the covering fraction for quasars from Prochaska et al. (2014), we restrict the sample to $z < 2.5$ where the Prochaska et al. (2014) sample closely follows the redshift-luminosity trend seen in the $z \approx 1$ samples (see the left panel of Figure 1).

With the correlation between Mg II absorption incidence and quasar luminosity in mind, we search for any additional dependence of Mg II absorption on redshift. To do so, we plot the covering fraction at $d < 200$ kpc of the luminous quasars as a function of redshift after resampling to mimic the projected distance distribution of the Prochaska et al. (2014) quasar sample in the right panel of Figure 4. At $z < 1$ and $z = 1 - 2$, the luminous quasars probed in Mg II exhibit covering fractions of $\kappa_{\text{Mg II}} = 0.55^{+0.09}_{-0.10}$ and $0.64^{+0.08}_{-0.10}$ at $d < 200$ kpc, consistent with no evolution between $z < 1$ and $z = 1 - 2$. The corresponding covering fraction for the $z \approx 2.2$ sample from Prochaska et al. (2014) is $\kappa = 0.76 \pm 0.12$, consistent with the covering fractions found for the $z < 1$ quasars at the level of 1.3σ . The increase from $\kappa_{\text{Mg II}} = 0.53^{+0.11}_{-0.12}$ at $z < 1$ to $\kappa = 0.76^{+0.07}_{-0.13}$ at $z \approx 2.2$ is suggestive, but a larger sample of quasars at $z \approx 2$ is required to investigate further. In addition, optical spectra of background sightlines toward quasars at $z < 2.5$ can provide constraints on Mg II absorption which would eliminate

³ The galaxy sample from Chen et al. (2010a) is based on a sample of $L \approx L_*$ galaxies at $z \lesssim 0.2$, but the scaling relations in Chen et al. (2010b) remain valid at $z < 2$ (Lovegrove & Simcoe 2011; Chen 2012; Liang & Chen 2014).

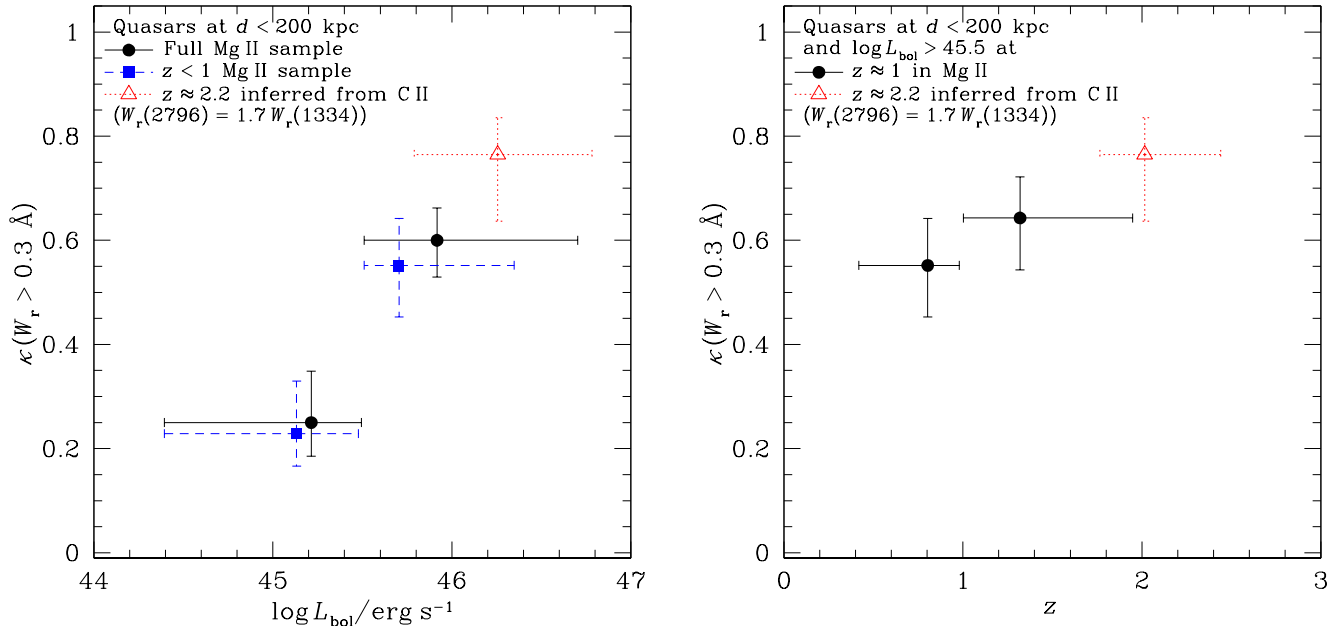


Figure 4. *left:* Covering fraction at $d < 200$ kpc of Mg II absorption systems of $W_r(2796) > 0.3 \text{ \AA}$ as a function bolometric luminosity of the foreground quasars. To isolate the correlation with luminosity from possible redshift evolution, we also show the covering fraction as a function of bolometric luminosity with the quasar sample restricted to $z < 1$ in blue. This redshift restriction is chosen so that the median redshift of the luminous quasars matches that of the low-luminosity quasars. *right:* Covering fraction at $d < 200$ for quasars of $\log L_{\text{bol}}/\text{erg s}^{-1} > 45.5$ as a function of redshift. In both panels, the vertical error bars mark 68% confidence intervals estimated from binomial statistics and the horizontal error bars mark the full range contributing to each bin. In both panels, the Mg II quasar sample is resampled to mimic the projected distance distribution of the $z \approx 2.2$ sample from Prochaska et al. (2014) (red).

the additional systematic uncertainty in converting between Mg II and C II absorption equivalent widths.

3.2 Kinematics

To characterize the kinematics of the Mg II absorption systems around quasars, we plot histograms of the radial velocity differences between the quasars and Mg II systems in the left panel of Figure 5. The radial velocity histograms are characterized by a core that is consistent with the velocity spread found around galaxies ($\sigma \approx 150 \text{ km s}^{-1}$; Chen et al. 2010a), but 29 out of 67 Mg II components (43%) are found at radial velocity differences with $|\Delta v| > 300 \text{ km s}^{-1}$ compared to 2 out of 47 galaxies (4%) in Chen et al. (2010a). Ten of 29 quasars with narrow-line redshifts and detected Mg II absorption are found to have Mg II absorption at $|\Delta v| = 300 - 1500 \text{ km s}^{-1}$ (34%) indicating that the majority of the large velocity differences are not the result of the uncertainties in broad-line based quasar redshifts (see the top left panel of Figure 5). Such large velocity differences are found among both high- and low-luminosity quasars, though the sample of low-luminosity quasars with Mg II absorption is small (see the bottom left panel of Figure 5).

In addition to large radial velocity differences, six quasars in the SDSS sample are found to have multiple, resolved Mg II absorption complexes spread over hundreds to thousands of km s^{-1} in the background quasar spectrum. The complex kinematics found for these six quasars are visualized in the right panel of Figure 5. The Mg II doublet

members are separated by a wavelength difference that corresponds to $\Delta v = 770 \text{ km s}^{-1}$, creating the potential for confusion between absorber kinematics and the weaker doublet member. To avoid this confusion in visualizing the systems of multiple Mg II absorption complexes, we fit the Mg II absorption using the VPFIT package and plot the data after dividing by the fit for the $\lambda 2803$ doublet member. We note that each absorption “complex” in the SDSS spectra would likely be resolved into multiple components in high resolution spectra.

3.3 Narrow, associated absorption systems

A few percent of optically selected quasars exhibit narrow, “associated” absorption-line systems ($z_{\text{abs}} \approx z_{\text{qso}}$) along the sightline to the quasar itself (e.g. Weymann et al. 1979; Wild et al. 2008; Vanden Berk et al. 2008). Associated absorption-line systems could arise in gas associated with the quasar, the interstellar medium of the quasar host, or the interstellar/circum-galactic medium of neighboring galaxies, but the ionizing radiation from the quasar is expected to photoevaporate Mg II absorbing clouds out to distances of ≈ 1 Mpc along the quasar sightline (Hennawi & Prochaska 2007; Wild et al. 2008). A recent comparison between quasars with narrow, associated Mg II absorption and a control sample of redshift and i -band magnitude matched quasars without associated absorption found that quasars with associated Mg II absorption exhibit slightly enhanced dust extinction ($E(B - V) \approx 0.03$) and a 50 – 70% enhancement in [O II] emission (Shen & Ménard 2012).

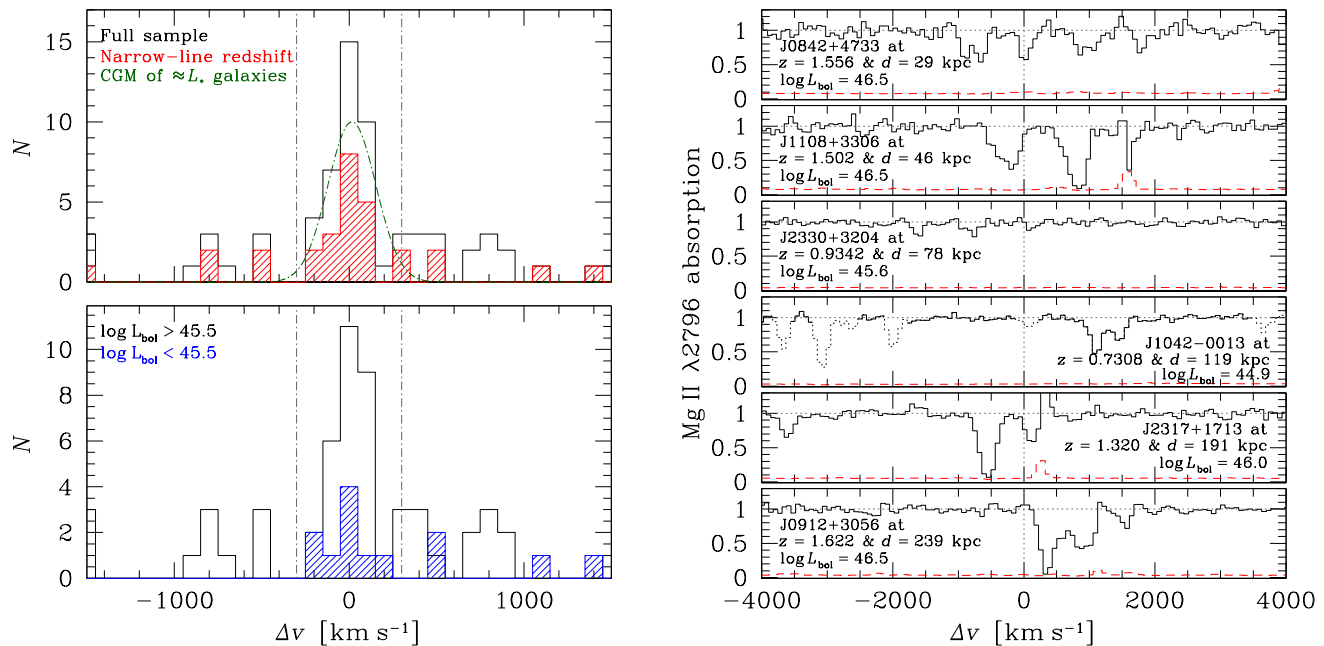


Figure 5. *left:* Histograms of the radial velocity differences between the quasar systemic redshifts and Mg II component redshifts at $\Delta v < 1500 \text{ km s}^{-1}$. The *top* panel shows the full Mg II sample in black, quasars with narrow-line redshifts in shaded red, and the fit to galaxies from Chen et al. (2010a) in green dash-dot line. Vertical lines mark $\pm 300 \text{ km s}^{-1}$, the expected virial velocity of a typical quasar host halo at $z = 1.0$. The *bottom* panel shows the radial velocity histogram for the high- and low-luminosity quasars in black and blue filled histogram respectively. *right:* Kinematic structure seen in absorption toward six foreground quasars observed with resolved velocity structure in SDSS spectra of the background quasar. The panels are labelled with the foreground quasar name, redshift, projected distance, and bolometric luminosity. Quasar redshifts from narrow lines are shown to four decimal places and those from broad lines are shown to three. To prevent confusion between kinematic structure and the weaker Mg II doublet member, we model the Mg II doublet observed in the SDSS spectra and plot the data divided by the model for the $\lambda 2803$ doublet member.

A search within our foreground quasar sample identifies four luminous and six low-luminosity quasars with associated ($|\Delta v| < 1500 \text{ km s}^{-1}$) narrow Mg II absorption systems along the foreground quasar sightline. Two of these four luminous quasars are found to have Mg II absorption systems detected in the background quasar spectra at $d = 150 - 300 \text{ kpc}$, consistent with expectations from the general high-luminosity quasar sample. None of the six low-luminosity quasars with associated absorption systems are found to have Mg II systems in the background quasar spectra at $d = 180 - 275 \text{ kpc}$, also consistent with expectations from the general, low-luminosity quasar sample. Though the sample of quasars with associated Mg II absorption and constraints on transverse Mg II absorption from background quasars is small, these results suggest that the large-scale halo gas contents of quasars with associated absorption are not radically different from those found in the general quasar population.

4 DISCUSSION

Using a sample of 195 quasars at $z \approx 1$ with constraints on Mg II absorption from background quasars at projected distances of $d < 300 \text{ kpc}$ from the SDSS, we characterized the cool gas contents of quasar host halos as a function of projected distance, quasar luminosity, and redshift. Our main findings are the following:

(i) Luminous quasars of $\log L_{\text{bol}}/\text{erg s}^{-1} > 45.5$ exhibit enhanced Mg II absorption relative to low-luminosity

quasars and inactive galaxies of similar mass at projected distances of $d < 300 \text{ kpc}$.

(ii) The absorbing gas near quasars exhibits complex kinematics with 30 – 40% of components found at $|\Delta v| = 300 - 1500 \text{ km s}^{-1}$ from the quasar systemic redshift. and

(iii) The incidence of cool gas absorption around luminous quasars does not evolve strongly with redshift between $z \approx 1$ and $z \approx 2.2$.

In this section, we discuss the possible origins of the extended Mg II absorbing gas near quasars, correlation with luminosity, and complex kinematics. Finally, we briefly consider possible avenues of future research.

Galaxies of $L \approx L_*$ at $z \lesssim 0.2$ exhibit high Mg II covering fractions out to a gaseous radius that is observed to scale with stellar mass according to $R_{\text{Mg II}} \propto M_*^{0.28}$ (Chen et al. 2010b) and comparisons with CGM absorption at higher redshift suggest that the low-redshift scaling relations remain valid at $z \lesssim 2$ (e.g. Lovegrove & Simcoe 2011; Chen 2012; Liang & Chen 2014). Since quasars are thought to reside in massive galaxies of $L \gtrsim L_*$, previous studies (e.g. Farina et al. 2014; Prochaska et al. 2014) suggested that the high incidence of C II and Mg II absorption observed at impact parameters of $d = 100 - 200 \text{ kpc}$ from quasars are the result of mass scaling of the CGM. In this scenario, the absorption traces the “normal” halo gas of inactive galaxies with masses similar to quasar hosts. However, the expected Mg II absorption incidence from inactive galaxies with masses similar to quasar hosts ($\log M_*/M_\odot \approx 11$ based on the cluster-

ing measurement from Shen et al. (2013b) and stellar-to-halo mass relation from Behroozi et al. (2013)) is significantly lower than the covering fraction observed around luminous quasars (see the right panel of Figure 3). Moreover, quasar luminosity and host halo mass are only weakly (if at all) correlated (e.g. Shen et al. 2013b) so the observed correlation between quasar luminosity and Mg II absorption cannot be explained by mass scaling.

Finally, the large velocity differences observed between the quasar and absorber redshifts (30–40% of absorption at $|\Delta v| = 300 - 1500 \text{ km s}^{-1}$) and complex kinematics seen in some sightlines (see Figure 5) are inconsistent with gas gravitationally bound to a halo with the mean mass of quasar hosts ($\log M_h/M_\odot = 12.8$; Shen et al. 2013b) which have inferred halo virial velocities of $\approx 300 \text{ km s}^{-1}$. However, clustering measurements constrain the mean mass of quasar hosts, not the overall host halo mass distribution (see discussion in White et al. 2012), and the large fraction of absorption at $|\Delta v| = 300 - 1500 \text{ km s}^{-1}$ could be explained if $\approx 30 - 40\%$ of quasars reside in halos with larger masses. To evaluate this possibility, we measure the radial velocity differences observed between quasars with narrow-line redshifts and Mg II absorption systems, correct for line-of-sight projection by multiplying by $\sqrt{3}$, and find a population averaged velocity dispersion of 1000 km s^{-1} between the quasars and absorbing gas. The halo mass corresponding to a virial velocity of 1000 km s^{-1} is $\log M_h/M_\odot = 14.4$. Such massive halos are three orders-of-magnitude less abundant than those of $\log M_h/M_\odot = 12.8$ (Tinker et al. 2008) making it unlikely that a substantial fraction of quasars reside in such massive systems. Direct confirmation of this conclusion will require redshift surveys to characterize the environments of quasars with constraints on halo gas properties from background sightlines.

The high Mg II gas covering fractions, correlation with quasar luminosity, and kinematics can be explained if the Mg II absorbing gas is the result of:

- (i) the CGM of neighboring galaxies at $\gtrsim 1 \text{ Mpc}$ scales but at projected distances of $d \lesssim 300 \text{ kpc}$,
- (ii) feedback from luminous quasars, or
- (iii) debris from the galaxy interactions and mergers thought to trigger luminous quasars.

In the following subsections, we discuss each of these possibilities in turn.

4.1 Mg II absorption from galaxies neighboring the quasar host

Large scale quasar-quasar (e.g. White et al. 2012) and quasar-galaxy (e.g. Shen et al. 2013b) clustering measurements indicate that quasars reside in massive halos that trace over-dense regions of the Universe. Consequently, the CGM of galaxies in neighboring halos at distances of $\gtrsim 1 \text{ Mpc}$ from the quasar but projected distances of $\lesssim 300 \text{ kpc}$ could contribute to the Mg II absorption covering fractions and explain the large radial velocity differences often observed between the quasar and absorber redshifts.

To evaluate the expected covering fraction from neighboring galaxies, we use four UV-bright quasars at $z = 0.3 - 0.6$ with highly complete redshift surveys of galaxies of $r_{\text{AB}} < 23$ from Chen & Mulchaey (2009); John-

son et al. (2013); and Johnson et al. (in prep). These surveys reveal the presence of galaxies with redshifts within $|\Delta v| < 1500 \text{ km s}^{-1}$ of the quasar redshift at projected distances of $d \lesssim 300 \text{ kpc}$ that could potentially contribute to the Mg II absorption observed around quasars at similar projected distances (see left panel of Figure 6). We estimate the expected contribution to the covering fraction observed around quasars from these neighboring galaxies using the covering fraction and luminosity scaling measurements from Chen et al. (2010a). In this calculation, we do not include galaxies more luminous than $M_B = -22.2$ since such luminous galaxies exhibit reduced incidence of Mg II absorption compared to galaxies of $L \approx L_*$ (Gauthier et al. 2010).

The expected Mg II covering fractions from neighboring galaxies can explain a significant portion of the Mg II absorption observed around quasars at $d < 300 \text{ kpc}$ (see right panel of Figure 6). Moreover, neighboring galaxies are often at $|\Delta v| \approx 300 - 1500 \text{ km s}^{-1}$ from the quasar, potentially explaining the kinematics observed in Mg II absorption. We note, however, that the sample of quasars with available deep redshift surveys is small (4 quasars) and, consequently, the estimated covering fraction from neighboring galaxies suffers from significant and poorly quantified sampling uncertainties.

If a substantial portion of the Mg II absorption observed around quasars traces the CGM of neighboring galaxies in other host halos at Mpc scales, then the correlation between quasar luminosity and Mg II absorption would imply a correlation between quasar luminosity and quasar-galaxy clustering. However, studies of quasar-quasar and quasar-galaxy clustering found no correlation between quasar luminosity and clustering on Mpc scales (e.g. Croom et al. 2005; Myers et al. 2007; White et al. 2012; Shen et al. 2013b). In addition, recent observations of projected quasar-photometric galaxy pair counts find no evidence for a correlation with quasar luminosity (Padmanabhan et al. 2009; Zhang et al. 2013; Scott et al. 2015). We note that some studies of quasar-photometric galaxy pair counts find excess counts at $d < 300 \text{ kpc}$ for luminous quasars (Serber et al. 2006), but this excess is attributed to galaxies in the quasar host halo and the excess is not observed on larger scales.

The lack of correlation between quasar luminosity and clustering are in tension with expectations from the observed correlation between Mg II covering fraction and quasar luminosity if a substantial portion of the absorption arises in neighboring halos on Mpc scales, in apparent contradiction with the covering fraction estimate shown in the right panel of Figure 6. This discrepancy can be explained by the proximity effect in which the UV light from the quasar photo-evaporates the cool halo gas of galaxies out to Mpc scales. Indeed, galaxies at $\Delta v < 3000 \text{ km s}^{-1}$ from quasars exhibit significantly reduced cool halo gas content compared to the general galaxy population (e.g. Pascarelle et al. 2001).

4.2 Mg II absorption due to quasar feedback

Radio-loud, lobe-dominated quasars (class FR II; Fanaroff & Riley 1974) are known to drive powerful outflows at both high and low redshift (e.g. Nesvadba et al. 2008; Fu & Stockton 2009). However, only a small fraction quasars are radio-loud and lobe-dominated (e.g. Urry & Padovani 1995; Ivezić et al. 2002), so radio-mode feedback alone cannot be

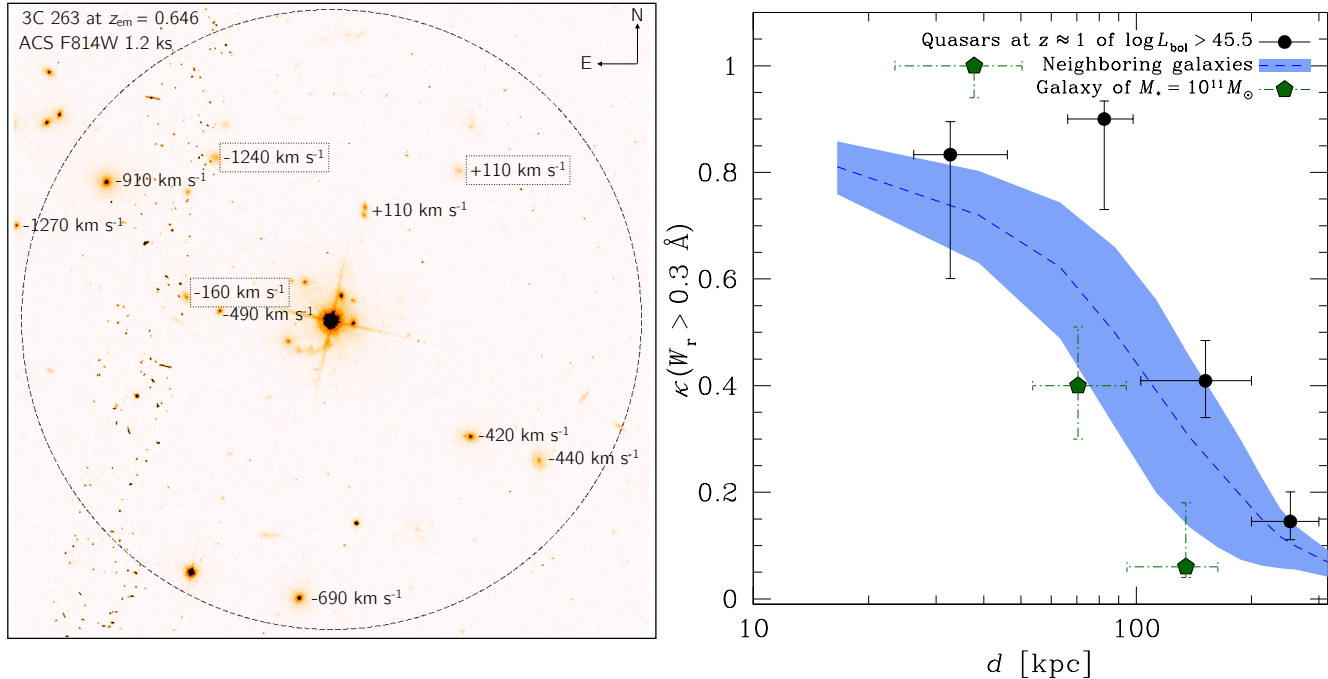


Figure 6. *left:* The galaxy environments near a luminous quasar (3C 263 at $z = 0.646$) with available deep redshift surveys targeting galaxies of $r_{AB} < 23$. Galaxies with secure redshifts and within $|\Delta v| < 1500 \text{ km s}^{-1}$ of the quasar redshift are labelled with Δv and star-forming galaxies are highlighted with dotted black outline. A dashed black circle of 150 kpc in radius centered on the quasar is shown for scale. The image is a stack of two 600 second exposures from the Advanced Camera for Surveys on the *Hubble Space Telescope* (PI: Mulchaey; PID: 13024) taken with the F814W filter with offsets between exposures to fill the gap between the ACS detectors. Cosmic ray removal is not possible in regions with coverage in only one exposure and these regions are visible as $5''$ wide stripes with high cosmic ray contamination. *right:* Covering fraction for absorption systems with $W_r(2796) > 0.3 \text{ \AA}$ as a function of projected distance for luminous quasars (black solid line) compared to expectations from a galaxy of $M_*/M_\odot = 11$ (green dash-dot line), and expected incidence due to neighbors of the quasar host (blue dashed line). The mean expected incidence due to neighbors is based on four UV-bright quasars with available deep galaxy redshift surveys and the light blue band represents the estimated uncertainty in the mean. We note, however, that with such a small sample size, uncertainty due to sampling are both large and poorly quantified.

responsible for the observed correlation between Mg II absorption and luminosity.

Recent observations of spatially resolved [O III] emission around luminous, radio-quiet, obscured (Type 2) quasars revealed the presence of surprisingly spherical gaseous nebulae that are both spatially ($\approx 30 \text{ kpc}$) and kinematically ($\approx 1000 \text{ km s}^{-1}$) extended (Greene et al. 2012; Liu et al. 2013a,b). Similar structures are observed in [O III] emission around luminous, radio-quiet, unobscured (Type 1) quasars (Liu et al. 2014) like those studied in this work. These observations are most naturally explained as fast outflows with wide opening angles driven by radio-quiet quasars (also see Zakamska & Greene 2014).

The quasar driven outflows observed in emission on scales of $\approx 30 \text{ kpc}$ may naturally explain the high incidence and complex kinematics of Mg II absorption around quasars if the outflows persist to larger distances but with gas densities that are too low to be observed in collisionally excited emission lines. An outflow with velocity $v_{\text{out}} = 1000 \text{ km s}^{-1}$ at 15 kpc from the host galaxy nucleus could reach distances of ≈ 100 (200) kpc in $\approx 10^8$ (2×10^8) years assuming that the outflow decelerates due to the gravitational potential of the host halo. The timescales required to reach 100–200 kpc from the host halo are comparable to the high end of quasar lifetime estimates (10^8 years; Martini 2004). Moreover, these

fast, quasar driven outflows are observed to be effective at luminosities of $\log L_{\text{bol}}/\text{erg s}^{-1} \gtrsim 45.5$ (e.g. Veilleux et al. 2013; Zakamska & Greene 2014) and could therefore explain the observed correlation between extended Mg II absorption and quasar luminosity.

In the outflow scenario, the Mg II absorbing gas represents cool clumps entrained in a hotter outflowing medium (e.g. Costa et al. 2015). Indeed, observations of outflows from both quasars and ultra-luminous infrared galaxies reveal copious quantities of highly ionized gas traced by CIV and OVI absorption (Arav et al. 2013; Martin et al. 2015). However, in the one foreground quasar with published high resolution background quasar spectroscopy, cool gas traced by C II absorption is found spread over 700 km s^{-1} but little absorption from more highly ionized species is found (Prochaska & Hennawi 2009). The low ionization state of the gas in this system ($N(\text{C II})/N(\text{C IV}) > 10$) is inconsistent with expectations from cool gas entrained in a quasar driven outflow, suggesting that quasar driven outflows alone cannot universally explain the high absorption covering fractions and complex kinematics observed around quasars.

Alternatively, the gas kinematics and ionization state can be understood if feedback from luminous quasars drives the pre-existing halo gas to large velocities, far in excess of the sound speed. Such fast bulk motions could lead to an en-

hanced fraction of gas with sufficiently high densities to cool and produce Mg II absorbing clumps. In this way, feedback from the quasar could convert halo gas generally observed in high ionization states at projected distances less than the virial radius (e.g. O VI; Chen & Mulchaey 2009; Tumlinson et al. 2011; Johnson et al. 2015) to lower-ionization states observable in Mg II absorption. Feedback from luminous quasars therefore represents a viable scenario for explaining the cool halo gas properties around quasar hosts including kinematics, correlation with luminosity, and enhanced covering fractions relative to inactive galaxies of similar masses.

4.3 Mg II absorption from tidal debris

Luminous quasars are thought to be fueled by gas supplied during galaxy mergers while the gas required to fuel less luminous AGN can be supplied by more secular processes (e.g. Hopkins & Hernquist 2009). The high incidence of absorbing gas around quasars and correlation with luminosity can be explained if the gas traces debris from the galaxy mergers that can trigger luminous AGN. Tidal debris can obtain velocities that exceed the escape velocity of the host halo (e.g. Toomre & Toomre 1972), possibly explaining the kinematics observed in absorption. The low ionization state ($N(\text{C II})/N(\text{C IV}) > 10$) observed in the one available quasar with high resolution background spectroscopy (Prochaska & Hennawi 2009) is consistent with the ionization state found in Magellanic Stream sightlines with similar H I column densities (Fox et al. 2014). Finally, deep 21-cm observations of the M81/M82 group reveal that relic gas from galaxy interactions can extend to cover large areas, possibly explaining the high Mg II covering fractions observed out to scales of $\lesssim 200$ kpc around luminous quasars. Tidal debris therefore represents a viable possibility for explaining observed Mg II absorption properties around quasars. We note, however, that it is not clear that tidal debris alone can explain the large fraction (30 – 40%) of Mg II absorption components found at radial velocities of $|\Delta v| > 300 \text{ km s}^{-1}$.

4.4 Future prospects

The high covering fraction of Mg II absorption observed around quasars, correlation with luminosity, and complex kinematics observed in our SDSS sample are not consistent with the absorption expected from inactive galaxies with masses similar to typical quasar hosts. In addition, clustering measurements imply that high- and low-luminosity quasars are hosted by halos of similar mean masses (Shen et al. 2013b) implying that the correlation between cool gas covering fraction and quasar luminosity is not the result of simple mass scaling of the circum-galactic medium. Together, these observations imply that a substantial portion of the Mg II absorbing gas does not originate in the “normal” halo gas of the quasar hosts. The high covering fraction, correlation with luminosity, and complex kinematics can be explained if the absorbing gas is the result of: (1) the CGM of neighboring galaxies on Mpc scales, (2) feedback from luminous quasars, or (3) relics from the interactions thought to trigger luminous quasars. The first of these

scenarios is in tension with the lack of correlation between quasar luminosity and clustering on Mpc scales (e.g. Serber et al. 2006; Shen et al. 2013b). The remaining two scenarios make distinct predictions that can be tested with additional observations.

If a substantial fraction of the Mg II absorbing gas is the result of quasar feedback, then we expect the cool gas absorption to be correlated with the presence of extended outflows observed in [O III] emission (e.g. Greene et al. 2012).

If, on the other hand, the Mg II absorbing gas arises in relics from the mergers that are thought to trigger luminous quasars, then the absorption would be correlated with the presence of disturbed host morphologies and nearby tidal remnants. At $z \approx 1$, searching for such interaction signatures requires the high resolution imaging capabilities of the *Hubble Space Telescope*.

ACKNOWLEDGEMENTS

It is a pleasure to thank Jenny Greene and Claude-Andr e Faucher-Gigu ere for lively discussion and insights that helped shape this paper. We are grateful to Yun-Hsin Huang for discussion of the software used for the absorption measurements and to Cameron Liang for suggestions that improved the presentation of data in the figures throughout the paper. In addition, we are grateful to the referee, Joe Hennawi, who provided constructive and substantive suggestions that helped improve the paper.

SDJ gratefully acknowledges funding from a National Science Foundation Graduate Research Fellowship and from the Brinson Foundation. JSM and HWC acknowledge partial support for this work from grant HST-GO-13024.001-A.

Funding for SDSS-III has been provided by the Alfred P. Sloan Foundation, the Participating Institutions, the National Science Foundation, and the U.S. Department of Energy Office of Science. The SDSS-III web site is <http://www.sdss3.org/>. SDSS-III is managed by the Astrophysical Research Consortium for the Participating Institutions of the SDSS-III Collaboration including the University of Arizona, the Brazilian Participation Group, Brookhaven National Laboratory, Carnegie Mellon University, University of Florida, the French Participation Group, the German Participation Group, Harvard University, the Instituto de Astrof sica de Canarias, the Michigan State/Notre Dame/JINA Participation Group, Johns Hopkins University, Lawrence Berkeley National Laboratory, Max Planck Institute for Astrophysics, Max Planck Institute for Extraterrestrial Physics, New Mexico State University, New York University, Ohio State University, Pennsylvania State University, University of Portsmouth, Princeton University, the Spanish Participation Group, University of Tokyo, University of Utah, Vanderbilt University, University of Virginia, University of Washington, and Yale University.

Based in part on observations made with the NASA/ESA Hubble Space Telescope, obtained from the data archive at the Space Telescope Science Institute. STScI is operated by the Association of Universities for Research in Astronomy, Inc. under NASA contract NAS 5-26555.

This research made use of NASA’s Astrophysics Data System (ADS) and the NASA/IPAC Extragalactic Database (NED) which is operated by the Jet Propulsion Laboratory,

California Institute of Technology, under contract with the National Aeronautics and Space Administration.

REFERENCES

- Agertz O., Kravtsov A. V., 2015, *ApJ*, 804, 18
- Alam S., Albareti F. D., Allende Prieto C., Anders F., Anderson S. F., Andrews B. H., Armengaud E., Aubourg É., Bailey S., Bautista J. E., et al., 2015, *ArXiv e-prints*
- Antonucci R., 1993, *ARAA*, 31, 473
- Arav N., Borguet B., Chamberlain C., Edmonds D., Danforth C., 2013, *MNRAS*, 436, 3286
- Behroozi P. S., Wechsler R. H., Conroy C., 2013, *ApJ*, 770, 57
- Benson A. J., Bower R. G., Frenk C. S., Lacey C. G., Baugh C. M., Cole S., 2003, *ApJ*, 599, 38
- Bergeron J., Stasińska G., 1986, *AAP*, 169, 1
- Bolton A. S., Schlegel D. J., Aubourg É., Bailey S., Bhardwaj V., Brownstein J. R., Burles S., Chen Y.-M., Dawson K., Eisenstein D. J., Gunn J. E., Knapp G. R., Loomis C. P., Lupton R. H., Maraston C., Muna D., Myers A. D., Olmstead M. D., Padmanabhan N., Pâris I., Percival W. J., Petitjean P., Rockosi C. M., Ross N. P., Schneider D. P., Shu Y., Strauss M. A., Thomas D., Tremonti C. A., Wake D. A., Weaver B. A., Wood-Vasey W. M., 2012, *AJ*, 144, 144
- Bordoloi R., Lilly S. J., Knobel C., Bolzonella M., Kampanczyk P., et al., 2011, *ApJ*, 743, 10
- Bordoloi R., Tumlinson J., Werk J. K., Oppenheimer B. D., Peoples M. S., Prochaska J. X., Tripp T. M., Katz N., Davé R., Fox A. J., Thom C., Ford A. B., Weinberg D. H., Burchett J. N., Kollmeier J. A., 2014, *ApJ*, 796, 136
- Boroson T., 2005, *AJ*, 130, 381
- Borthakur S., Heckman T., Strickland D., Wild V., Schiminovich D., 2013, *ApJ*, 768, 18
- Bowen D. V., Blades J. C., Pettini M., 1995, *ApJ*, 448, 634
- Bowen D. V., Hennawi J. F., Ménard B., Chelouche D., Inada N., Oguri M., Richards G. T., Strauss M. A., Vanden Berk D. E., York D. G., 2006, *ApJL*, 645, L105
- Carswell R. F., Webb J. K., 2014, *VPFIT: Voigt profile fitting program. Astrophysics Source Code Library*
- Carswell R. F., Webb J. K., Baldwin J. A., Atwood B., 1987, *ApJ*, 319, 709
- Chen H.-W., 2012, *MNRAS*, 427, 1238
- Chen H.-W., Helsby J. E., Gauthier J.-R., Shtetman S. A., Thompson I. B., Tinker J. L., 2010a, *ApJ*, 714, 1521
- Chen H.-W., Lanzetta K. M., Webb J. K., 2001, *ApJ*, 556, 158
- Chen H.-W., Lanzetta K. M., Webb J. K., Barcons X., 1998, *ApJ*, 498, 77
- Chen H.-W., Mulchaey J. S., 2009, *ApJ*, 701, 1219
- Chen H.-W., Wild V., Tinker J. L., Gauthier J.-R., Helsby J. E., Shtetman S. A., Thompson I. B., 2010b, *ApJL*, 724, L176
- Conroy C., Wechsler R. H., 2009, *ApJ*, 696, 620
- Costa T., Sijacki D., Haehnelt M. G., 2015, *MNRAS*, 448, L30
- Croom S. M., Boyle B. J., Shanks T., Smith R. J., Miller L., Outram P. J., Loaring N. S., Hoyle F., da Ángela J., 2005, *MNRAS*, 356, 415
- Di Matteo T., Springel V., Hernquist L., 2005, *Nature*, 433, 604
- Eisenstein D. J., Weinberg D. H., Agol E., Aihara H., Allende Prieto C., Anderson S. F., Arns J. A., Aubourg É., Bailey S., Balbinot E., et al., 2011, *AJ*, 142, 72
- Fabian A. C., 2012, *ARAA*, 50, 455
- Fanaroff B. L., Riley J. M., 1974, *MNRAS*, 167, 31P
- Farina E. P., Falomo R., Decarli R., Treves A., Kotilainen J. K., 2013, *MNRAS*, 429, 1267
- Farina E. P., Falomo R., Scarpa R., Decarli R., Treves A., Kotilainen J. K., 2014, *MNRAS*, 441, 886
- Faucher-Giguère C.-A., Hopkins P. F., Kereš D., Muratov A. L., Quataert E., Murray N., 2015, *MNRAS*, 449, 987
- Feigelson E. D., Nelson P. I., 1985, *ApJ*, 293, 192
- Ford A. B., Oppenheimer B. D., Davé R., Katz N., Kollmeier J. A., Weinberg D. H., 2013, *MNRAS*, 432, 89
- Fox A. J., Wakker B. P., Barger K. A., Hernandez A. K., Richter P., Lehner N., Bland-Hawthorn J., Charlton J. C., Westmeier T., Thom C., Tumlinson J., Misawa T., Howk J. C., Haffner L. M., Ely J., Rodriguez-Hidalgo P., Kumari N., 2014, *ApJ*, 787, 147
- Fu H., Stockton A., 2009, *ApJ*, 690, 953
- Fumagalli M., Hennawi J. F., Prochaska J. X., Kasen D., Dekel A., Ceverino D., Primack J., 2014, *ApJ*, 780, 74
- Gabor J. M., Davé R., 2012, *MNRAS*, 427, 1816
- Gaskell C. M., 1982, *ApJ*, 263, 79
- Gauthier J.-R., Chen H.-W., Tinker J. L., 2010, *ApJ*, 716, 1263
- Greene J. E., Zakamska N. L., Smith P. S., 2012, *ApJ*, 746, 86
- Hennawi J. F., Prochaska J. X., 2007, *ApJ*, 655, 735
- , 2013, *ApJ*, 766, 58
- Hennawi J. F., Prochaska J. X., Burles S., Strauss M. A., Richards G. T., Schlegel D. J., Fan X., Schneider D. P., Zakamska N. L., Oguri M., Gunn J. E., Lupton R. H., Brinkmann J., 2006, *ApJ*, 651, 61
- Hewett P. C., Wild V., 2010, *MNRAS*, 405, 2302
- Hopkins P. F., Hernquist L., 2009, *ApJ*, 694, 599
- Hummels C. B., Bryan G. L., Smith B. D., Turk M. J., 2013, *MNRAS*, 430, 1548
- Isobe T., Feigelson E. D., Nelson P. I., 1986, *ApJ*, 306, 490
- Ivezić Ž., Menou K., Knapp G. R., Strauss M. A., Lupton R. H., Vanden Berk D. E., Richards G. T., Tremonti C., Weinstein M. A., Anderson S., Bahcall N. A., Becker R. H., Bernardi M., Blanton M., Eisenstein D., Fan X., Finkbeiner D., Finlator K., Frieman J., Gunn J. E., Hall P. B., Kim R. S. J., Kinkhabwala A., Narayanan V. K., Rockosi C. M., Schlegel D., Schneider D. P., Strateva I., SubbaRao M., Thakar A. R., Voges W., White R. L., Yanny B., Brinkmann J., Doi M., Fukugita M., Hennessy G. S., Munn J. A., Nichol R. C., York D. G., 2002, *AJ*, 124, 2364
- Johnson S. D., Chen H.-W., Mulchaey J. S., 2013, *MNRAS*, 434, 1765
- , 2015, *MNRAS*, 449, 3263
- Kravtsov A., Vikhlinin A., Meshcheryakov A., 2014, *ArXiv e-prints*
- Kravtsov A. V., Borgani S., 2012, *ARAA*, 50, 353
- Li Y., Bryan G. L., 2014, *ApJ*, 789, 54
- Liang C. J., Chen H.-W., 2014, *MNRAS*, 445, 2061
- Liu G., Zakamska N. L., Greene J. E., 2014, *MNRAS*, 442, 1303

- Liu G., Zakamska N. L., Greene J. E., Nesvadba N. P. H., Liu X., 2013a, *MNRAS*, 430, 2327
- , 2013b, *MNRAS*, 436, 2576
- Lovegrove E., Simcoe R. A., 2011, *ApJ*, 740, 30
- Martin C. L., Dijkstra M., Henry A., Soto K. T., Danforth C. W., Wong J., 2015, *ApJ*, 803, 6
- Martini P., 2004, *Coevolution of Black Holes and Galaxies*, 169
- Mathes N. L., Churchill C. W., Kacprzak G. G., Nielsen N. M., Trujillo-Gomez S., Charlton J., Muzahid S., 2014, *ApJ*, 792, 128
- Meiksin A., Bolton J. S., Tittley E. R., 2015, *ArXiv e-prints*
- Myers A. D., Brunner R. J., Nichol R. C., Richards G. T., Schneider D. P., Bahcall N. A., 2007, *ApJ*, 658, 85
- Nesvadba N. P. H., Lehnert M. D., De Breuck C., Gilbert A. M., van Breugel W., 2008, *AAP*, 491, 407
- Netzer H., 2015, *ArXiv e-prints*
- Oke J. B., Gunn J. E., 1983, *ApJ*, 266, 713
- Padmanabhan N., White M., Norberg P., Porciani C., 2009, *MNRAS*, 397, 1862
- Pascarelle S. M., Lanzetta K. M., Chen H.-W., Webb J. K., 2001, *ApJ*, 560, 101
- Prochaska J. X., Hennawi J. F., 2009, *ApJ*, 690, 1558
- Prochaska J. X., Hennawi J. F., Simcoe R. A., 2013, *ApJL*, 762, L19
- Prochaska J. X., Lau M. W., Hennawi J. F., 2014, *ApJ*, 796, 140
- Prochaska J. X., Weiner B., Chen H.-W., Mulchaey J., Cooksey K., 2011, *ApJ*, 740, 91
- Rahmati A., Schaye J., Bower R. G., Crain R. A., Furlong M., Schaller M., Theuns T., 2015, *ArXiv e-prints*
- Rao S. M., Turnshek D. A., Nestor D. B., 2006, *ApJ*, 636, 610
- Richards G. T., Lacy M., Storrie-Lombardi L. J., Hall P. B., Gallagher S. C., Hines D. C., Fan X., Papovich C., Vanden Berk D. E., Trammell G. B., Schneider D. P., Vestergaard M., York D. G., Jester S., Anderson S. F., Budavári T., Szalay A. S., 2006, *ApJS*, 166, 470
- Richards G. T., Vanden Berk D. E., Reichard T. A., Hall P. B., Schneider D. P., SubbaRao M., Thakar A. R., York D. G., 2002, *AJ*, 124, 1
- Rudie G. C., Steidel C. C., Shapley A. E., Pettini M., 2013, *ApJ*, 769, 146
- Rudie G. C., Steidel C. C., Trainor R. F., Rakic O., Bogosavljević M., Pettini M., Reddy N., Shapley A. E., Erb D. K., Law D. R., 2012, *ApJ*, 750, 67
- Schaye J., Dalla Vecchia C., Booth C. M., Wiersma R. P. C., Theuns T., Haas M. R., Bertone S., Duffy A. R., McCarthy I. G., van de Voort F., 2010, *MNRAS*, 402, 1536
- Schlafly E. F., Finkbeiner D. P., 2011, *ApJ*, 737, 103
- Schmidt M., Green R. F., 1983, *ApJ*, 269, 352
- Scott J. E., Rafiee A., Bechtold J., Ellingson E., Thibodeau C., Richmond M., 2015, *ApJ*, 800, 93
- Serber W., Bahcall N., Ménard B., Richards G., 2006, *ApJ*, 643, 68
- Shen S., Madau P., Guedes J., Mayer L., Prochaska J. X., Wadsley J., 2013a, *ApJ*, 765, 89
- Shen Y., McBride C. K., White M., Zheng Z., Myers A. D., Guo H., Kirkpatrick J. A., Padmanabhan N., Parejko J. K., Ross N. P., Schlegel D. J., Schneider D. P., Streblyanska A., Swanson M. E. C., Zehavi I., Pan K., Bizyaev D., Brewington H., Ebelke G., Malanushenko V., Malanushenko E., Oravetz D., Simmons A., Snedden S., 2013b, *ApJ*, 778, 98
- Shen Y., Ménard B., 2012, *ApJ*, 748, 131
- Shen Y., Richards G. T., Strauss M. A., Hall P. B., Schneider D. P., Snedden S., Bizyaev D., Brewington H., Malanushenko V., Malanushenko E., Oravetz D., Pan K., Simmons A., 2011, *ApJS*, 194, 45
- Sijacki D., Springel V., Di Matteo T., Hernquist L., 2007, *MNRAS*, 380, 877
- Springel V., Di Matteo T., Hernquist L., 2005, *MNRAS*, 361, 776
- Stocke J. T., Keeney B. A., Danforth C. W., Shull J. M., Froning C. S., et al., 2013, *ApJ*, 763, 148
- Stocke J. T., Keeney B. A., Danforth C. W., Syphers D., Yamamoto H., Shull J. M., Green J. C., Froning C., Savage B. D., Wakker B., Kim T.-S., Ryan-Weber E. V., Kacprzak G. G., 2014, *ApJ*, 791, 128
- Suresh J., Bird S., Vogelsberger M., Genel S., Torrey P., Sijacki D., Springel V., Hernquist L., 2015, *MNRAS*, 448, 895
- Tinker J., Kravtsov A. V., Klypin A., Abazajian K., Warren M., Yepes G., Gottlöber S., Holz D. E., 2008, *ApJ*, 688, 709
- Toomre A., Toomre J., 1972, *ApJ*, 178, 623
- Tripp T. M., Lu L., Savage B. D., 1998, *ApJ*, 508, 200
- Tumlinson J., Thom C., Werk J. K., Prochaska J. X., Tripp T. M., et al., 2013, *ApJ*, 777, 59
- Tumlinson J., Thom C., Werk J. K., Prochaska J. X., Tripp T. M., et al., 2011, *Science*, 334, 948
- Turner M. L., Schaye J., Steidel C. C., Rudie G. C., Strom A. L., 2014, *MNRAS*, 445, 794
- Tytler D., Fan X.-M., 1992, *ApJS*, 79, 1
- Urry C. M., Padovani P., 1995, *PASP*, 107, 803
- Vanden Berk D., Khare P., York D. G., Richards G. T., Lundgren B., Alsayyad Y., Kulkarni V. P., SubbaRao M., Schneider D. P., Heckman T., Anderson S., Crotts A. P. S., Frieman J., Stoughton C., Lauroesch J. T., Hall P. B., Meiksin A., Steffing M., Vanlandingham J., 2008, *ApJ*, 679, 239
- Veilleux S., Meléndez M., Sturm E., Gracia-Carpio J., Fischer J., González-Alfonso E., Contursi A., Lutz D., Poglitsch A., Davies R., Genzel R., Tacconi L., de Jong J. A., Sternberg A., Netzer H., Hailey-Dunsheath S., Verma A., Rupke D. S. N., Maiolino R., Teng S. H., Polisensky E., 2013, *ApJ*, 776, 27
- Vestergaard M., Wilkes B. J., 2001, *ApJS*, 134, 1
- Vogelsberger M., Genel S., Sijacki D., Torrey P., Springel V., Hernquist L., 2013, *MNRAS*, 436, 3031
- Wakker B. P., Savage B. D., 2009, *ApJS*, 182, 378
- Werk J. K., Prochaska J. X., Thom C., Tumlinson J., Tripp T. M., O'Meara J. M., Peebles M. S., 2013, *ApJS*, 204, 17
- Weymann R. J., Williams R. E., Peterson B. M., Turnshek D. A., 1979, *ApJ*, 234, 33
- White M., Myers A. D., Ross N. P., et al., 2012, *MNRAS*, 424, 933
- Wild V., Kauffmann G., White S., York D., Lehnert M., Heckman T., Hall P. B., Khare P., Lundgren B., Schneider D. P., vanden Berk D., 2008, *MNRAS*, 388, 227
- York D. G., Adelman J., Anderson Jr. J. E., et al., 2000, *AJ*, 120, 1579
- Zakamska N. L., Greene J. E., 2014, *MNRAS*, 442, 784

Zhang S., Wang T., Wang H., Zhou H., 2013, ApJ, 773,
175

Zhu G., Ménard B., 2013, ApJ, 770, 130

This paper has been typeset from a $\text{T}_{\text{E}}\text{X}/\text{L}^{\text{A}}\text{T}_{\text{E}}\text{X}$ file prepared
by the author.